

7N-05
198707
P-19

TECHNICAL NOTE

D-284

EFFECTS OF JET BILLOWING ON STABILITY OF
MISSILE-TYPE BODIES AT MACH 3.85

By Reino J. Salmi

Lewis Research Center
Cleveland, Ohio

NATIONAL AERONAUTICS AND SPACE ADMINISTRATION

WASHINGTON

June 1960

(NASA-TN-D-284) EFFECTS OF JET BILLOWING ON
STABILITY OF MISSILE-TYPE BODIES AT MACH
3.85 (NASA. Lewis Research Center) 19 p

N89-70813

Unclas
00/05 0198707

NATIONAL AERONAUTICS AND SPACE ADMINISTRATION

TECHNICAL NOTE D-284

EFFECTS OF JET BILLOWING ON STABILITY OF

MISSILE-TYPE BODIES AT MACH 3.85

By Reino J. Salmi

SUMMARY

The interference effects of a billowing jet on the forces and moments of two missile-type bodies were investigated in the NASA Lewis 2-by 2-foot Mach 3.85 wind tunnel. To simulate a rocket jet, pressurized nitrogen was exhausted from an annular sonic nozzle.

The results indicate that for both models the stability parameter $dC_m/d\alpha$ (rate of change of pitching-moment coefficient with angle of attack) in the region of zero angle of attack was favorably influenced by the interference resulting from separation due to jet billowing. Schlieren photographs are presented that show the separation due to the jet billowing at various pressure ratios and angles of attack.

INTRODUCTION

The exhaust jets of most rocket-powered missiles or airplanes become greatly underexpanded at high altitudes, causing the jet to billow out beyond the fuselage diameter. Experimental and theoretical investigations such as references 1 and 2 have defined the shape and size of jets exhausting into supersonic streams. The billowing jet (ref. 3) acts like a solid body of similar shape in interfering with the external flow over the vehicle. For the case of the airplane of reference 3, adverse interference effects on the longitudinal stability resulted from jet billowing.

The jet interference phenomenon is, basically, the problem of shock-wave - boundary-layer interactions. A shock wave is produced when the supersonic flow past the body meets the expanded jet plume. The pressure rise across the shock wave eventually becomes too great for the body boundary layer to surmount, and separation occurs. The phenomenon is similar to the separation on spikes protruding from blunt bodies as described in references 4 to 6 and the separation produced by forward-facing steps in a supersonic stream as shown in reference 7.

Of primary interest, of course, are the effects of jet billowing on the aerodynamic forces and moments of the vehicle. An investigation was made, therefore, to determine the magnitude and nature of the forces and moments due to jet billowing on two missile-type bodies. The models included a circular cylindrical configuration and one with a 6° flared afterbody. The tests were made in the NASA Lewis 2- by 2-foot Mach 3.85 wind tunnel, using an annular sonic jet at exit static-pressure ratios up to 3280 to simulate a rocket exhaust.

SYMBOLS

A	area
C_m	pitching-moment coefficient, $m/q_0 A l$
$dC_m/d\alpha$	rate of change of pitching-moment coefficient with angle of attack
C_N	normal force coefficient, $N/q_0 A$
$dC_N/d\alpha$	rate of change of normal force coefficient with angle of attack
d	diameter
g	annular nozzle gap
l	model length
m	pitching moment
N	normal force
p	static pressure
q	dynamic pressure
x	longitudinal distance from model nose
α	angle of attack
Subscripts:	
e	exit
p	plug
0	free-stream value

MODELS AND APPARATUS

Two missile-type models were investigated, one having a circular cylindrical afterbody and the other with a 6° flared skirt afterbody. Both had a common conical blunt nose. On the flared model, the flare originated at a point 71.4 percent aft of the nose, as shown by the model dimensions and construction details in figure 1.

Both models were of fineness ratio 6.8 based on the diameter of the cylindrical section. Photographs of the models installed in the tunnel are presented in figure 2.

A rocket exhaust was simulated with high-pressure nitrogen supplied to an annular sonic nozzle as shown in figure 1. This type of nozzle was used to obtain a high jet-exit static-pressure ratio with a limited chamber pressure. The normal force and pitching moment were obtained with strain gages located at two model stations.

The tests were conducted in the Lewis 2- by 2-foot Mach 3.85 wind tunnel at a free-stream Reynolds number of approximately 1.42×10^6 based on the model length. Data were obtained through an angle-of-attack range of $\pm 6^\circ$ and at jet-exit static-pressure ratios up to approximately 3280.

RESULTS AND DISCUSSION

The results obtained with the sonic annular jet are similar to those that would result from an actual rocket exhaust, although not necessarily at equivalent jet-exit static-pressure ratios. The forces on the model due to the jet-billowing interference result from the effects of shock-induced separation on the body. The separation angle and the pressure rise in the separated region depend on the Reynolds number and Mach number, whereas the extent of the separated region varies with the size and shape of the billowing jet. For a given region of separated flow over the missile body, the interference forces will be approximately equal regardless of the type of interference causing the separation. In reference 3, for example, a solid metal shield shaped to simulate an exiting air jet produced almost identical flow-separation characteristics at zero angle of attack.

The size and shape of the exiting jet are determined by the exit static-pressure ratio p_e/p_0 , the nozzle exit angle, the ratio of specific heats γ , and the exit Mach number. For any given engine, however, these quantities are relatively constant, except for the exit static-pressure ratio, which varies with altitude and combustion-chamber pressure.

The effects of jet-billowing interference on the static stability and normal force parameters are shown in figure 3. The results indicated that the stability parameter $dC_m/d\alpha$ was favorably influenced by the interference resulting from separation due to jet billowing, whereas previous results on an airplane-type configuration having tail surfaces indicated that jet-billowing interference effects were destabilizing. The difference in results for the unfinned body and the airplane configuration may well be expected, since the stabilizing effect of the horizontal tail can be greatly diminished if a major part of it is in the separated-flow region where the dynamic pressure is low and the flow direction less favorable.

In the case of the cylindrical model, the stability parameter $dC_m/d\alpha$ decreased almost linearly with increasing jet-exit static-pressure ratio and became negative at a pressure ratio of about 2500. The flared afterbody configuration was neutrally stable with the jet off and up to a jet pressure ratio of about 240. Between pressure ratios of about 240 and 1250, the stability increased to a maximum value at a pressure ratio of 600 and then decreased to zero. Because of nozzle failure, no force data were obtained for the flared model at pressure ratios above 1250. For both configurations, the normal force parameter $dC_N/d\alpha$ generally decreased with increasing jet pressure ratio. The variations of C_N and C_m with angle of attack were linear in the range investigated, and the data are not presented.

The center-of-pressure variations with jet static-pressure ratio are presented in figure 4. For the cylindrical model, a forward movement in the center of pressure from about 33 percent of the body length to about 27 percent occurred in the pressure-ratio range from jet off to about 200. The assumed center of gravity (center of volume of the cylindrical model) was located 53.3 percent aft of the nose.

Theoretical flow models of the separation due to forward-facing steps usually assume a uniform pressure in the separated region that is equal to the pressure rise associated with the separation angle. Although no data are presented because of measuring inaccuracies, pressure distributions along the model indicated that the pressures in the separated region increased gradually from the point of separation to the end of the body. It is possible that a vigorous circulatory flow existed in the separated regions to support such a pressure rise.

Schlieren photographs of the flow past the models at various jet pressure ratios and angles of attack are presented in figures 5 and 6. The separated regions due to the shock-wave - boundary-layer interaction moved forward with increasing jet-exit static-pressure ratio. The flow regions indicated by schlieren photographs are defined in figure 5(a). At high pressure ratios, the separated regions extended to the shoulder of the nose cone on both surfaces. As would be expected, the jet plumes were much larger on the lee side of the models at angle of attack.

CONCLUDING REMARKS

An experimental investigation of the interference effects of jet billowing on two missile-type configurations indicated that the static stability as measured by $dC_m/d\alpha$ in the region of zero angle of attack was favorably influenced when the jet-exit static-pressure ratio was increased for both cylindrical and flared afterbody models, whereas destabilizing effects of jet billowing had been observed previously on an airplane-type configuration having tail surfaces.

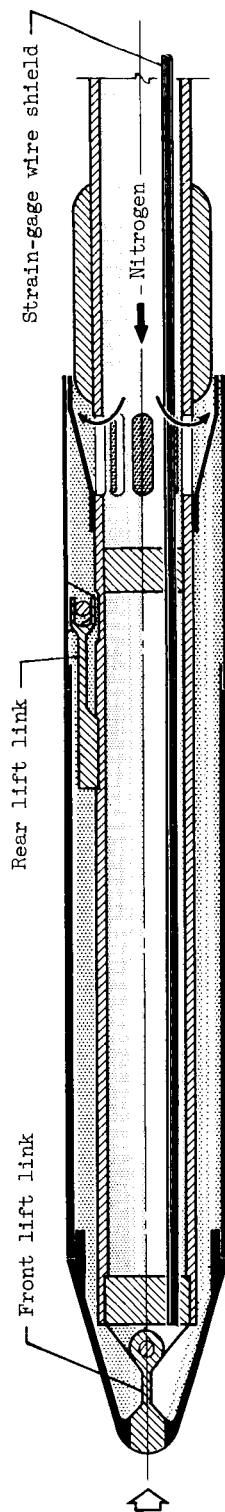
Lewis Research Center

National Aeronautics and Space Administration

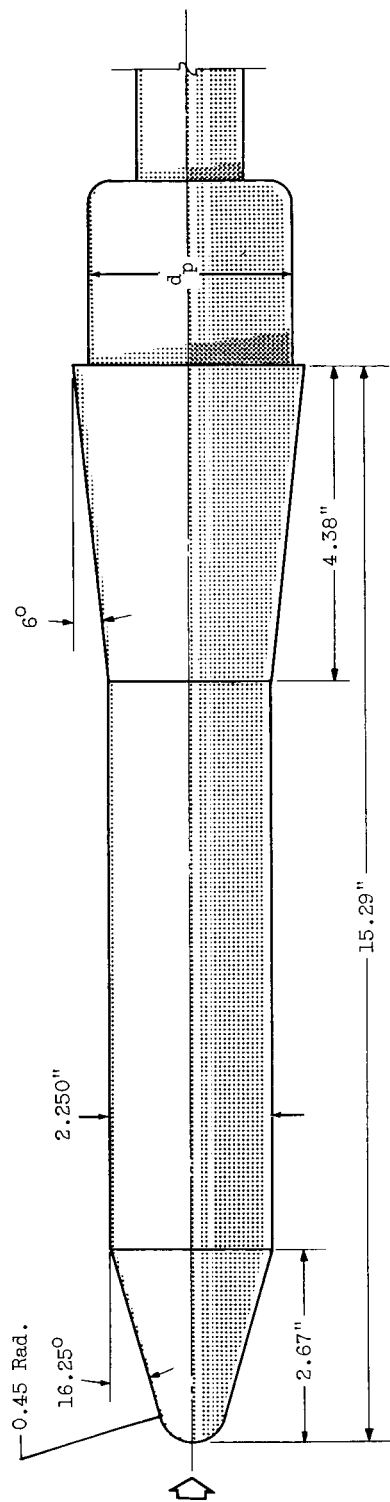
Cleveland, Ohio, March 4, 1960

REFERENCES

1. Love, Eugene S., and Grigsby, Carl E.: Some Studies of Axisymmetric Free Jets Exhausting from Sonic and Supersonic Nozzles Into Still Air and Into Supersonic Streams. NACA RM L54L31, 1955.
2. Englert, Gerald W.: Operational Method of Determining Initial Contour of and Pressure Field About a Supersonic Jet. NASA TN D-279, 1960.
3. Fetterman, David E., Jr.: Effects of Simulated Rocket-Jet Exhaust on Stability and Control of a Research-Type Airplane Configuration at a Mach Number of 6.86. NASA TM X-127, 1959.
4. Moeckel, W. E.: Flow Separation Ahead of Blunt Bodies at Supersonic Speeds. NACA TN 2418, 1951.
5. Moeckel, W. E.: Flow Separation Ahead of a Blunt Axially Symmetric Body at Mach Numbers 1.76 and 2.10. NACA RM E51I25, 1951.
6. Jones, Jim J.: Flow Separation from Rods Ahead of Blunt Noses at Mach Number 2.72. NACA RM L52EO5a, 1952.
7. Bernstein, Harry, and Brunk, William E.: Exploratory Investigation of Flow in the Separated Region Ahead of Two Blunt Bodies at Mach Number 2. NACA RM E55DO7b, 1955.

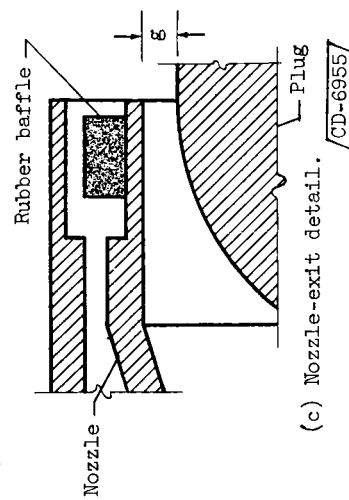


(a) Cross section of model with cylindrical afterbody.



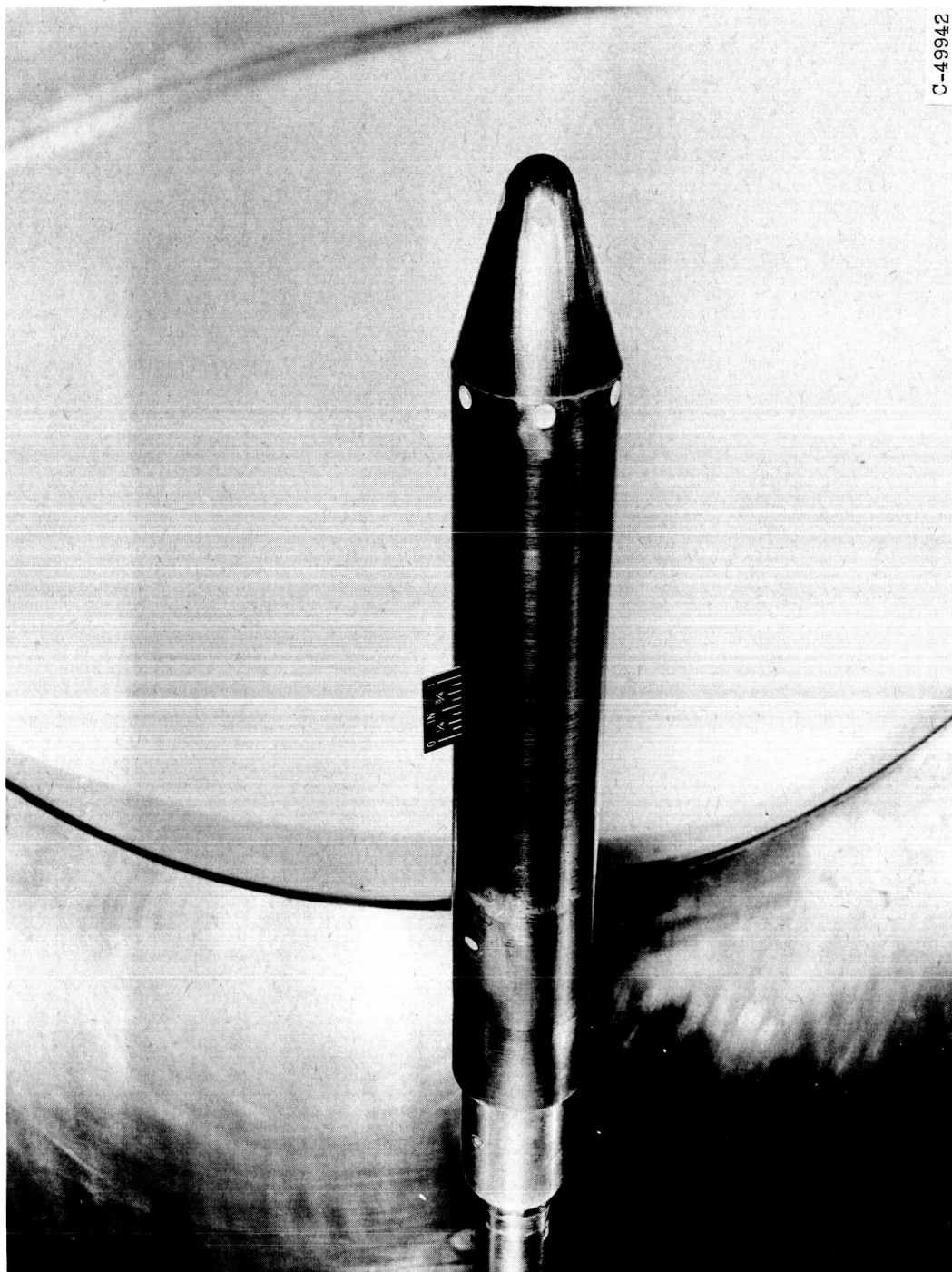
(b) Model with flared afterbody.

	Cylindrical model	Flared model
A_e , in.	0.446	0.492
d_p , in.	1.930	2.795
g , in.	.071	.055



(c) Nozzle-exit detail.

Figure 1. - Model geometry and details.



(a) Cylindrical afterbody.

Figure 2. - Model.



(b) Flared afterbody.

Figure 2. - Concluded. Model.

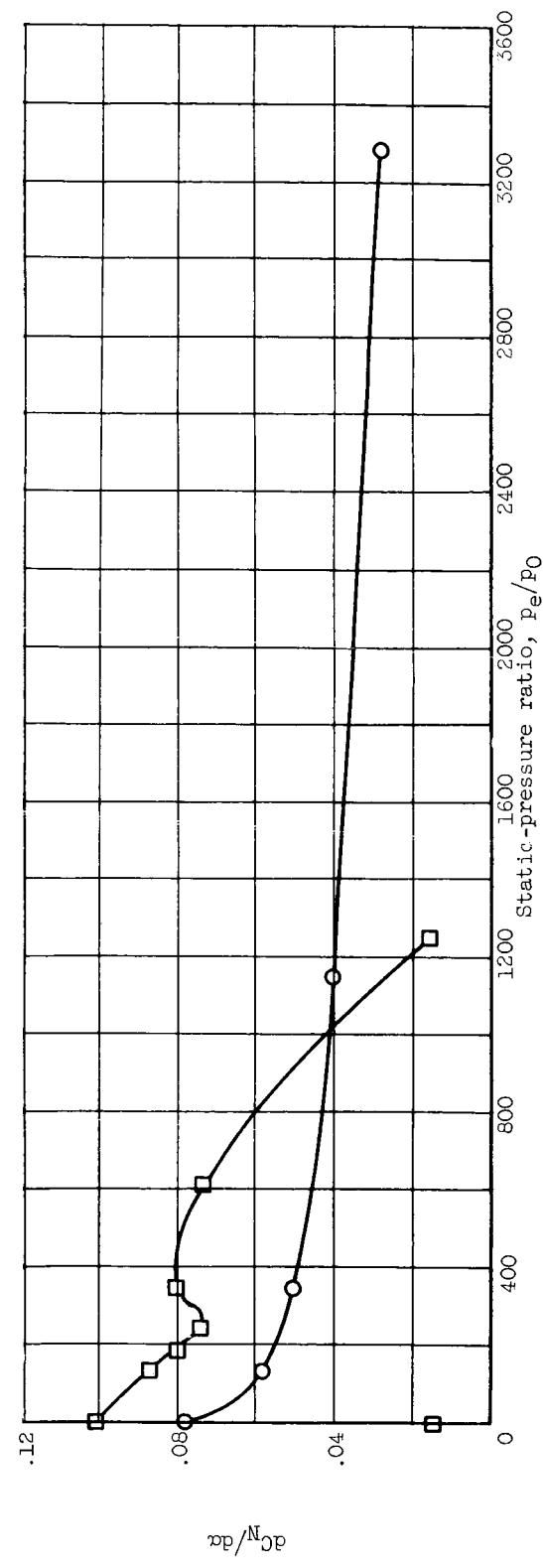
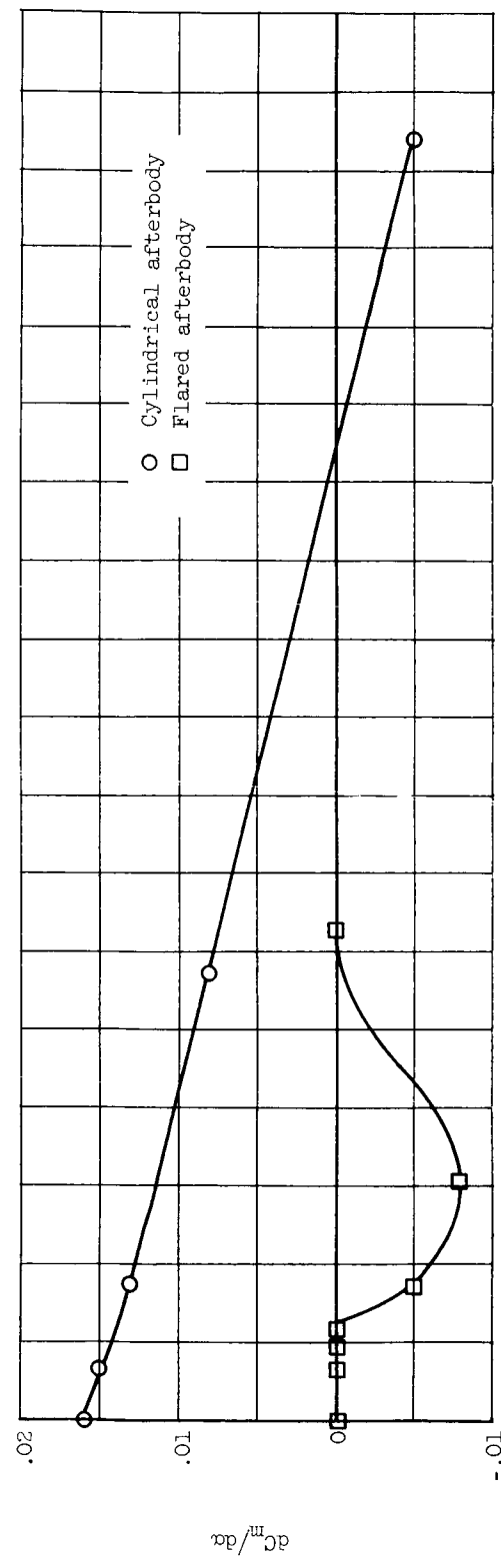


Figure 3. - Effect of jet-exit static-pressure ratio on longitudinal stability parameters.

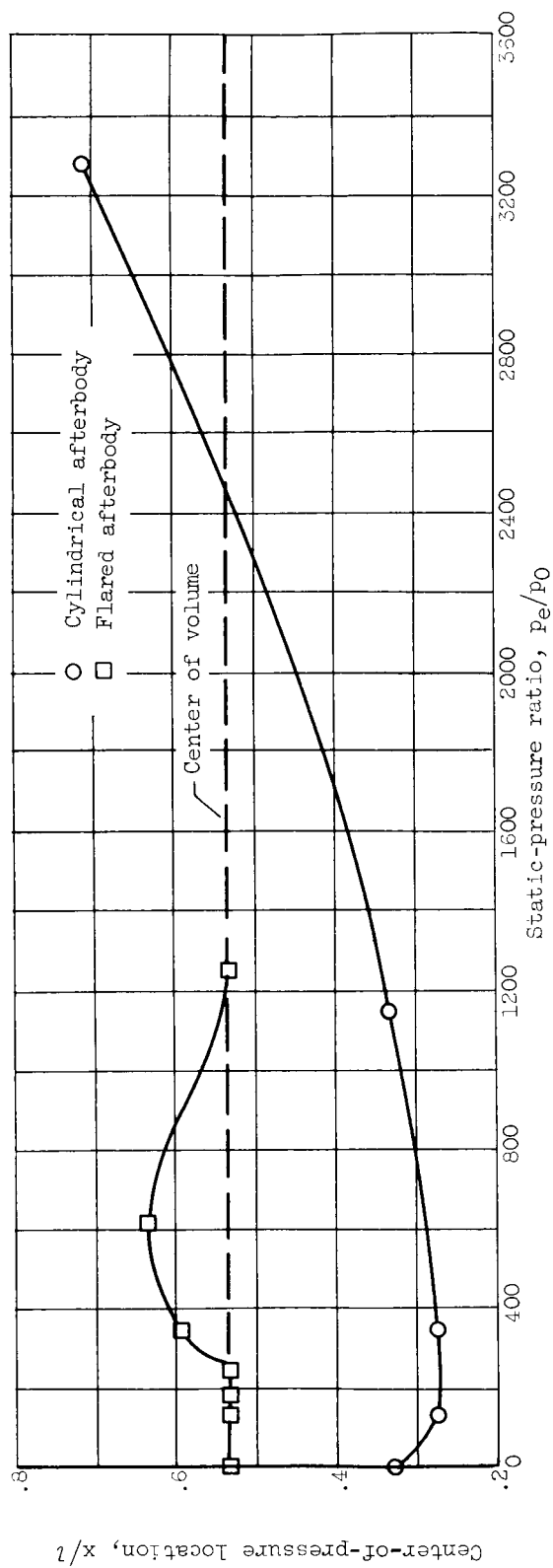
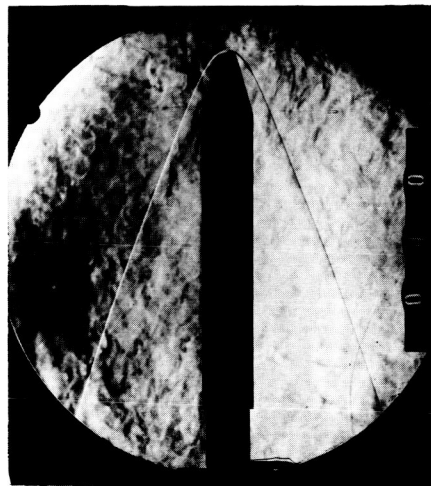
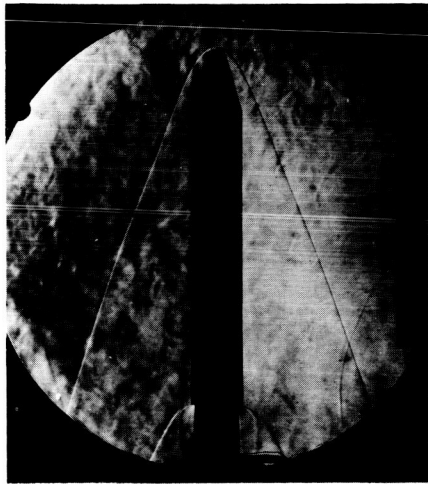


Figure 4. - Effect of jet-exit static-pressure ratio on center of pressure.



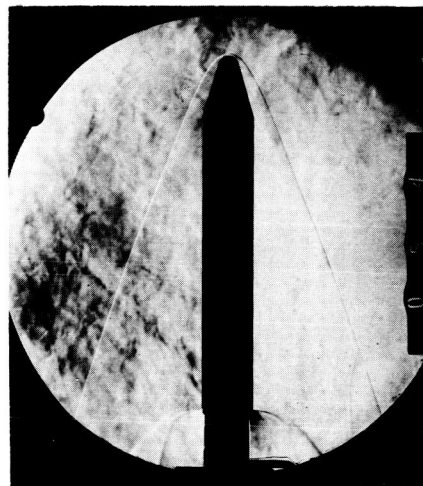
Jet off



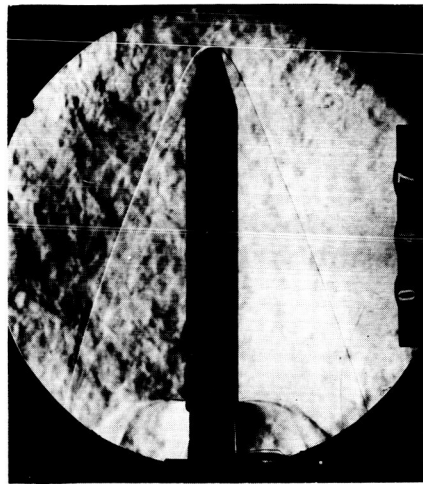
$p_e/p_0 \approx 130$



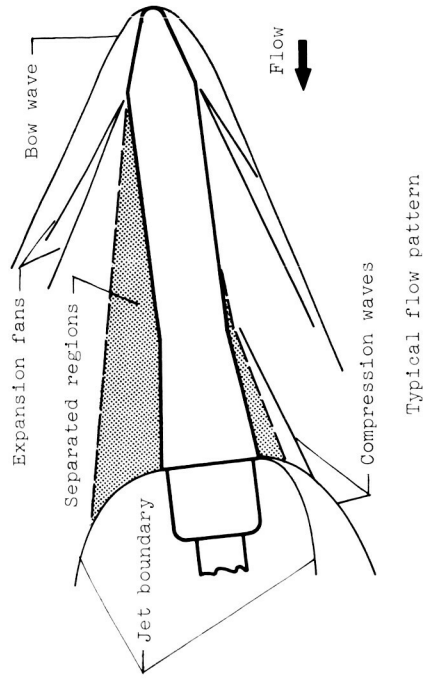
$p_e/p_0 \approx 345$



$p_e/p_0 \approx 1145$

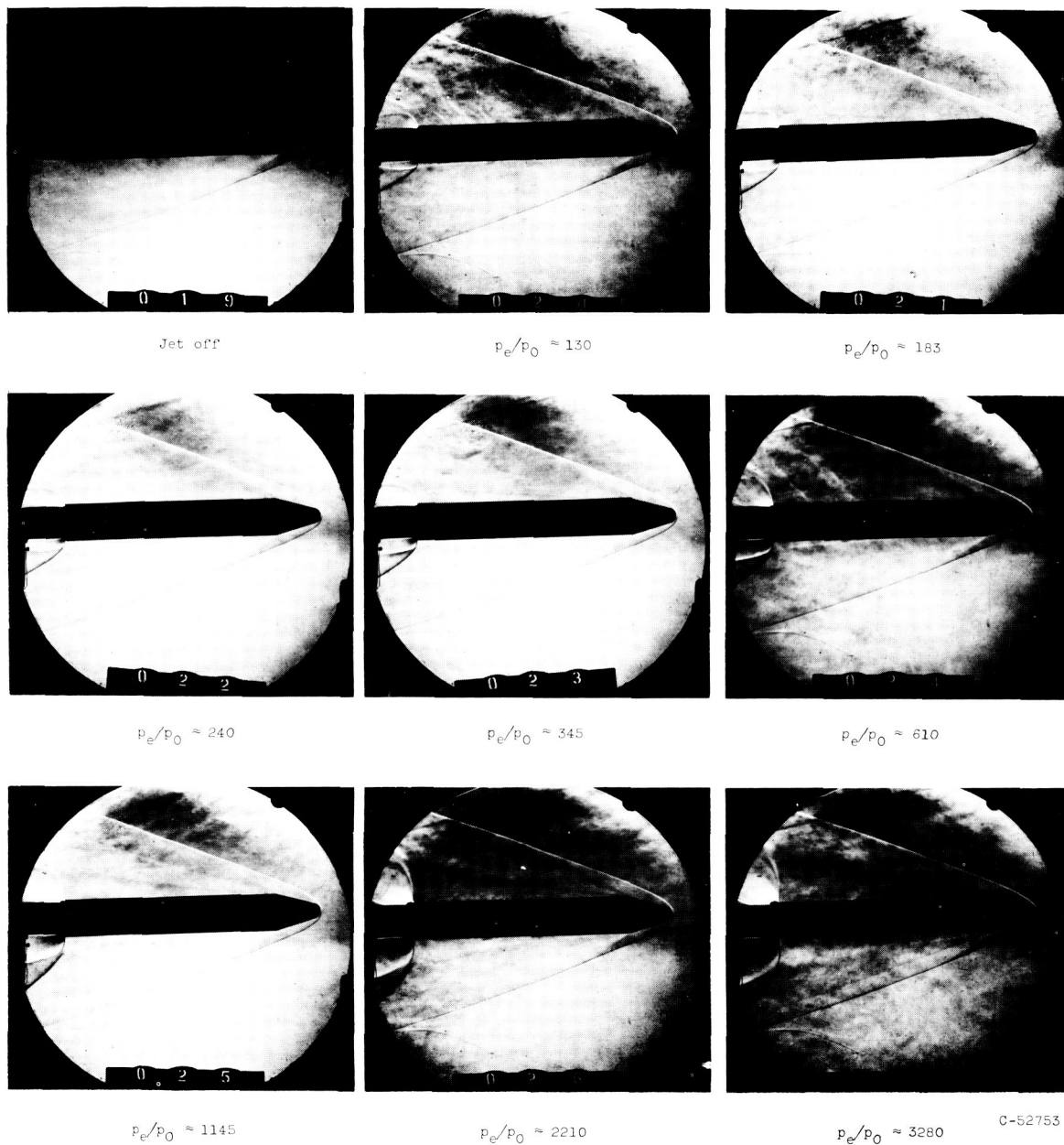


$p_e/p_0 \approx 3280$
C-52759



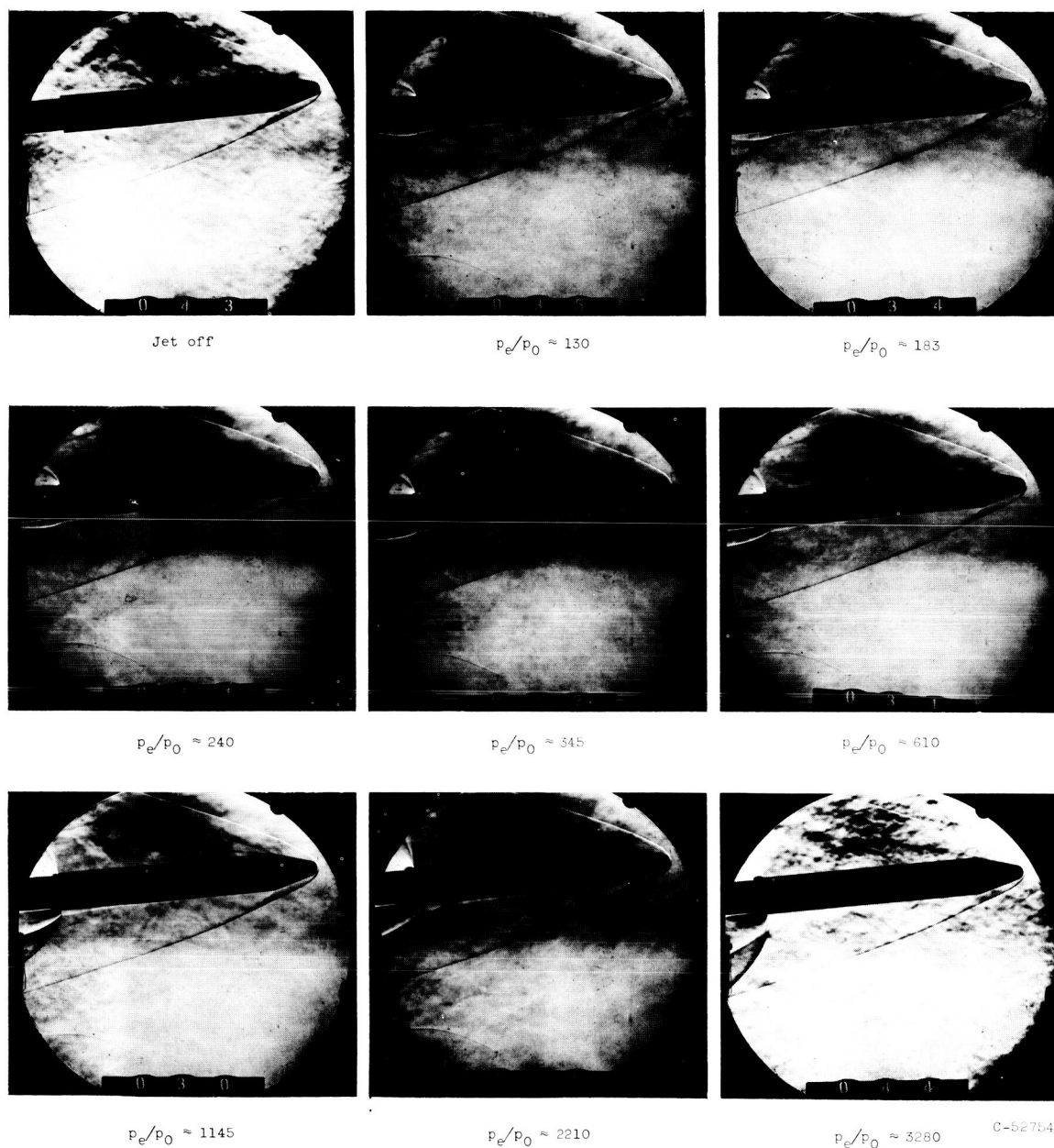
(a) Angle of attack, 0° .

Figure 5. - Schlieren photographs of cylindrical model at various jet-exit static-pressure ratios.



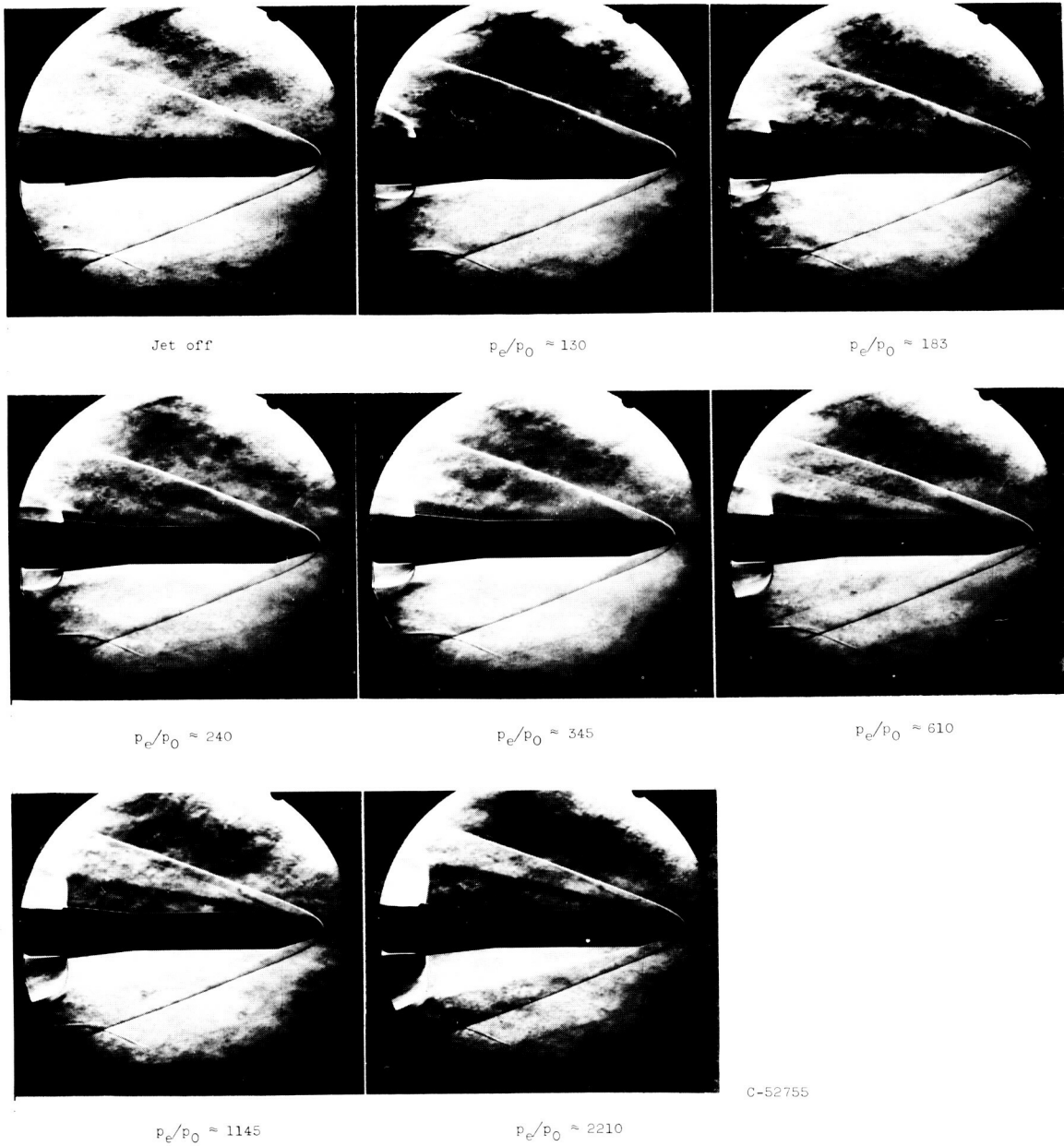
(b) Angle of attack, 2° .

Figure 5. - Continued. Schlieren photographs of cylindrical model at various jet-exit static-pressure ratios.



(c) Angle of attack, 6° .

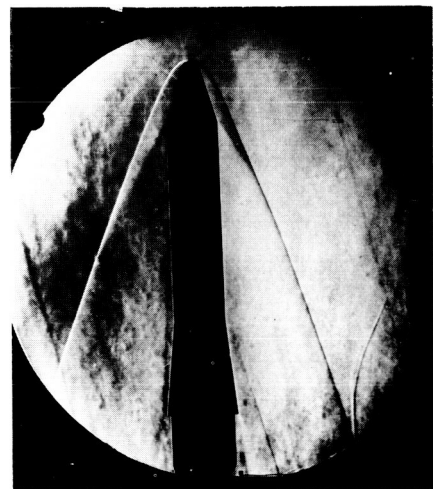
Figure 5. - Concluded. Schlieren photographs of cylindrical model at various jet-exit static-pressure ratios.



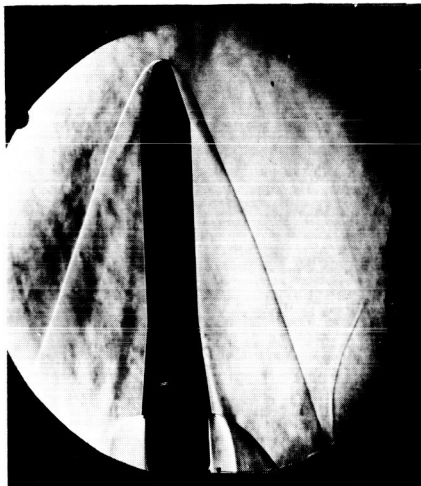
C-52755

(a) Angle of attack, 0° .

Figure 6. - Schlieren photographs of flared afterbody model at various jet-exit static-pressure ratios.



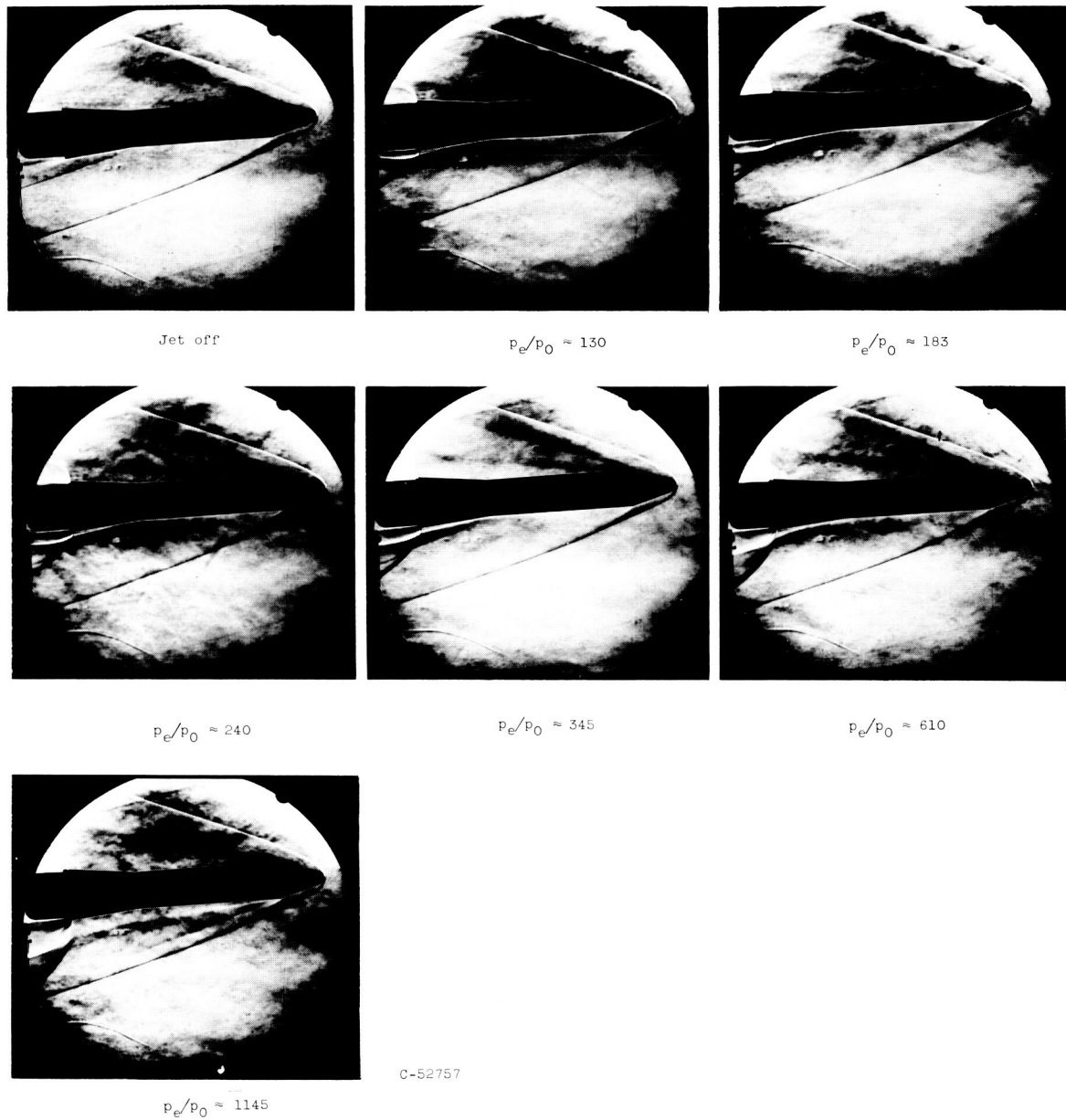
Jet off

 $p_e/p_0 \approx 130$  $p_e/p_0 \approx 183$  $p_e/p_0 \approx 240$  $p_e/p_0 \approx 345$

C-52756

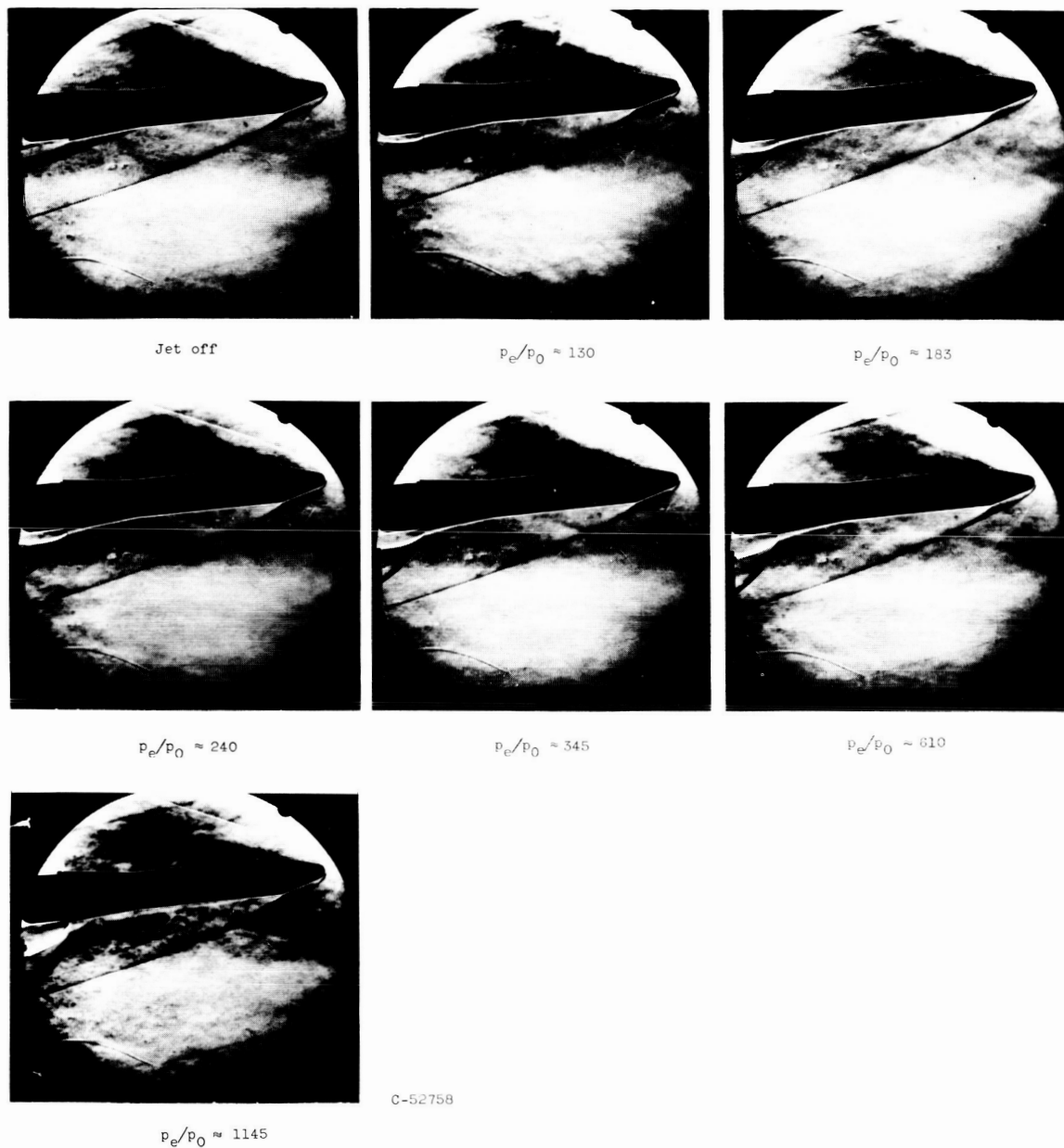
(b) Angle of attack, 2° .

Figure 6. - Continued. Schlieren photographs of flared afterbody model at various jet-exit static-pressure ratios.



(c) Angle of attack, 4° .

Figure 6. - Continued. Schlieren photographs of flared afterbody model at various jet-exit static-pressure ratios.



(d) Angle of attack, 6° .

Figure 6. - Concluded. Schlieren photographs of flared afterbody model at various jet-exit static-pressure ratios.